Decon in the log domain - practical considerations

Ohad Barak, Antoine Guitton and Shuki Ronen

ABSTRACT

We apply deconvolution in the log domain to marine seismic data. The inversion promotes sparsity. We compare the deconvolution results of using two types of regularizations: filter symmetry and filter length. We show that the regularizations aid in acquiring the correct shot waveform, and in sparsifying the data. An consideration that we can add to the inversion is the elimination of the marine acquisition notch frequency.

INTRODUCTION

In marine streamer acquisition, both the source and the receivers are at some depth. As a result, their reflection from the water surface generates "ghost" arrivals. These ghosts are recorded in addition to the primary path of energy propagation from source to reflector to receiver. This causes the recordings of the specular reflections to be in practice non-minimum phase wavelets, and more similar to Ricker wavelets, as most of the energy does not arrive at the onset of the wavelet. Since Ricker is a delayed zero-phase wavelet, predictive decon will have limited success on marine streamer data, as the inverse filter will have coefficients that increase with time. Additionally, the airgun typically employed as a source in marine surveys generates a low-frequency bubble, whose reverberations contaminate the recorded data.

Zhang et al. (2011) extended traditional deconvolution to non-minimum phase wavelets. Claerbout et al. (2011) replaced the unknown filter coefficients by lag coefficients in the log spectrum of the deconvolution filter. Given data $D(\omega)$, the deconvolved output r_t is:

$$r_t \;=\; \mathrm{FT}^{-1}\;\left[D(\omega)\;\exp\left(\sum_t u_t Z^t\right)\right] \tag{1}$$

where FT^{-1} is the inverse Fourier transform, and $Z = e^{i\omega}$. u_t are the log spectrum variables of the deconvolution filter. The source wavelet is the inverse of the exponent of these log variables. The positive lag coefficients correspond to the causal part of the wavelet, and the negative ones to the anticausal part.

Claerbout et al. (2012) introduced the concept of inverting for sparsity, with the added complication that seismic data is non-stationary but decreases in amplitude

over time. A gained residual $q_t = g_t r_t$ is sparsified using a hyperbolic penalty function $H(q_t)$, where g_t is a known gain function. The inversion finds the model parameters u_t which cause the gained residual q_t to be as sparse as possible. The purpose is to enhance frequencies where they promote sparsity, which is our assumption about the underlying geology. In addition they proposed two regularizations:

Symmetry regularization
The expected shot waveform is a zero-phase Ricker wavelet, ignoring the bubble which arrives later. Therefore, in the log spectral domain it is desirable to have only even parts of the filter coefficients u_t around the zero-lag. The symmetry regularization does this by incorporating the odd parts near zero-lag into the residual:

$$0 \approx \epsilon_1 \sum_\tau w_\tau (u_\tau - u_{-\tau}), \tag{2}$$

where u_τ are the coefficients at positive lags and $u_{-\tau}$ the coefficients at negative lags. w_τ is a weighting function that decreases from one to zero with increasing lag. Conceptually, the width of the weighting function should be just large enough to contain the Ricker wavelet of the data. ϵ_1 controls the degree to which this regularization affects the objective function.

Filter length regularization
The deconvolution filter's positive lags should include both the zero-phase Ricker wavelet of the reflections, and the wavelet of the bubble with its reverberations (which are caused by the implosion of water into the cavity generated by the airgun). The filter should not have large negative lags, beyond those needed for the anti-causal part of the Ricker wavelet. Therefore a filter length lag regularization is added to the residual

$$0 \approx \epsilon_2 \sum_\tau \left(c_\tau u_\tau + a_{-\tau} u_{-\tau} \right), \tag{3}$$

where c_τ is the weighting function for the positive lags. This function starts at zero for small positive lags, until the lag deemed to be sufficient to contain the bubble. $a_{-\tau}$ is the weighting function for the negative lags. This function is zero for small negative lags, and it ramps up from zero to one within a small time lag, since we do not expect anything before zero time other than the first lobe of the Ricker.

Additional considerations

Another consequence of the source and receiver ghost signals is the presence of notch frequencies. The particular frequency value in which a notch will occur depends on the time difference between the positive and negative lobes of the Ricker, and therefore on the depths of the source and receiver, and their offset:

$$f_n = \frac{V_w}{2d\cos(\theta)}, \tag{4}$$

where V_w is the water velocity, d is the depth and θ is the reflection angle. Since the sources and receivers are usually towed at a depth of only a few meters, the notch frequency is quite high (above 100Hz), and increases with offset. In order to see it in the spectrum of the data we would usually require a time sampling of 2ms.

The purpose of deconvolution is to separate out the parts of the data that are a result of acquisition from the parts that are a result of geology. Therefore, if the notch is visible in the spectrum of the data, we expect that after a successful deconvolution the notch will have been filled in.

In this paper, we show the results of applying this deconvolution method to various offsets of a marine streamer dataset, with and without regularizations. The code used is the same as in Claerbout et al. (2012), and was written by Antoine Guitton.

DECON RESULTS

Near offset

The dataset we used is a single 2D line from a marine streamer survey in the Gulf of Baja California (Lizzaralde et al., 2002). This line consists of 2298 shots. There were 480 receivers along the cable, and the group spacing was 12.5m. The nearest offset was 180m, and the farthest was 6180m.

Figure 1 is the near-offset section of the data. A gain of t^2 has been applied. Note the Ricker-like appearance of the reflections. Note also the bubble visible 200ms below the sea-bottom reflection. Other weaker bubble reverberations are within the section. A weak direct arrival of one of the bubble reverberations appears faintly at 500ms.

We ran two types of inversions:

1. Gained input deconvolution: Inversion is applied to data which was gained by t^2, and there is no gain applied to the residual ($g_t = t^0$).
2. Gained output deconvolution: Input data was not gained, but the residual was gained at each iteration of the inversion ($g_t = t^2$).

Additionally, for each gain type, we ran the inversion with and without regularizations, by setting the values of ϵ_1 and ϵ_2 in equations (2) and (3) accordingly.

Figure 2(a) shows the gained input deconvolution run without regularizations. Note that while the deconvolution has indeed spiked the reflections on the central lobe of the Ricker wavelet, the bubble is still visible, and the precursors are strong. Figure 2(b) is the gained output deconvolution run without regularizations. While the bubble seems to have been dealt with better in this section, the precursors above the sea-bottom reflection are stronger, and the entire section appears noisier. Figure

4(a) shows the shot-waveform estimated by the gained input deconvolution, and 4(b) is the one estimated by the gained output deconvolution. In each plot, the upper trace is the same as the lower trace, except that it has been clipped in order to enhance the smaller coefficients in the display. The smaller coefficients are important, since deconvolution is a division operation. Note how much more energy is in the anti-causal part of the shot-waveform in Figure 4(b) as compared to Figure 4(a). Both of them however show the main shot-waveform as a Ricker centered at zero-lag, and a bubble with its associated reverberations. This means that the inversion has indeed arrived at what we assumed to be the correct objective: in order to sparsify the data, the Ricker wavelet and the bubble must be removed.

Figure 3(a) is the gained input deconvolution run with the symmetry and filter length regularizations. Compared to Figure 2(a), the bubble is weaker, and so are the precursors. This can be further validated by comparing the precursors of the shot waveform in Figure 4(a) vs. Figure 4(c). Figure 3(b) is the gained output deconvolution run with the regularizations. Compared to Figure 3(a), the bubble is better eliminated. There is a slight difference in the estimated bubble in the shot-waveforms of Figures 4(c) and 4(d), and this is enough to cause the difference in bubble elimination. The precursors for the gained output deconvolution with regularization are the weakest, which is a direct result of forcing the filter length to be short.

Offset group

In this section, the purpose was to test whether utilizing more of the data will aid the inversion in acquiring the effective shot waveform, and therefore produce the sparsest result. We have seen that for the near offset section, even without regularization the estimated waveform was a Ricker wavelet. We now apply the inversion to a near-offset range, from 180m to 1180m.

Figure 5(a) is the result of applying the gained input deconvolution to the offset group without regularization, and then windowing out the near offset only for display. Compared to the same process applied to the near offset only (Figure 2(a)), the polarity of the reflections is incorrect, and the precursor is stronger. We can also see a low frequency precursors in the water. The deconvolution has spiked the Ricker on its second negative lobe.

Figure 5(b) is the result of applying the gained output deconvolution to the offset group without regularization. When compared with Figure 2(b), the polarity of the reflections is again wrong, but the precursor is weaker. The low-frequency precursor is visible here too. In this case, the deconvolution has spiked the Ricker on its first negative lobe.

The respective estimated shot waveforms are shown in Figures 7(a) and 7(b). Note the shift of the negative spike about the zero-lag in these two figures. Note also the low frequency (visible in the clipped traces) in the anti-causal part of the shot waveforms. These results show that for the range of offsets chosen here, requiring the

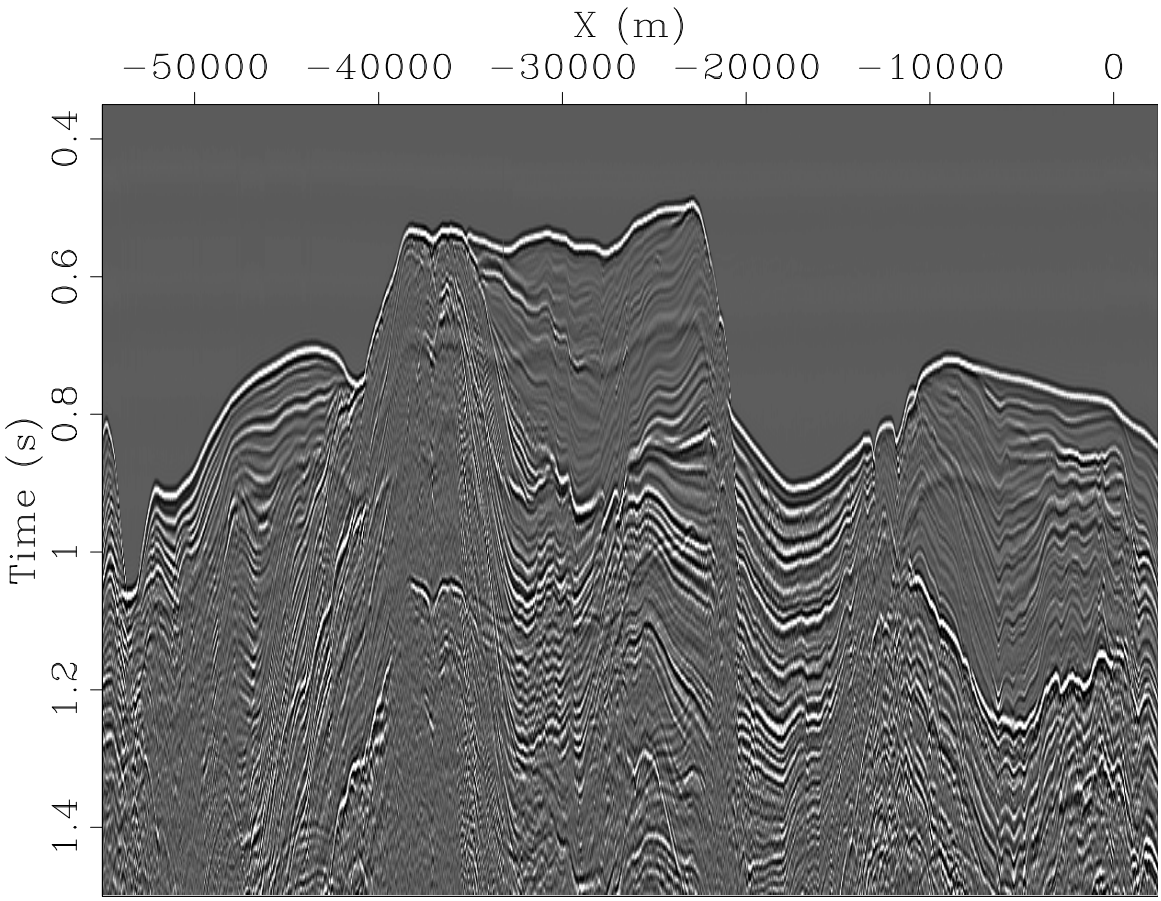

Figure 1: Gained near-offset section of Baja data. Offset is 180m. Note the Ricker-like appearance of the reflections, and the bubble around 200ms below the sea-bottom reflection. [**ER**]

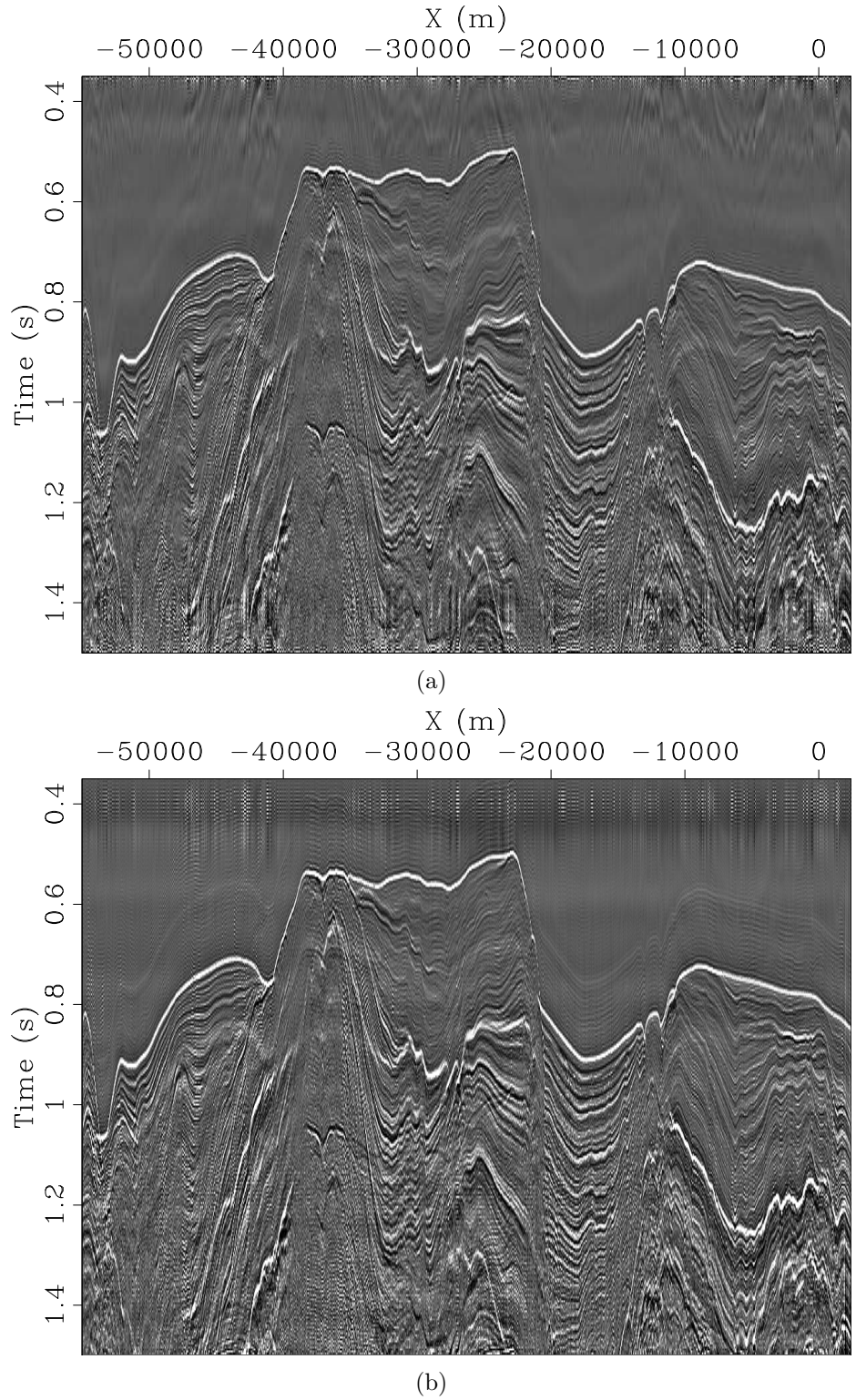

Figure 2: Deconvolution of the 180m offset only. (a) Gained input deconvolution without regularization. (b) Gained output deconvolution without regularization. Note how the Ricker wavelet has been spiked, and the strong precursors. [**ER**]

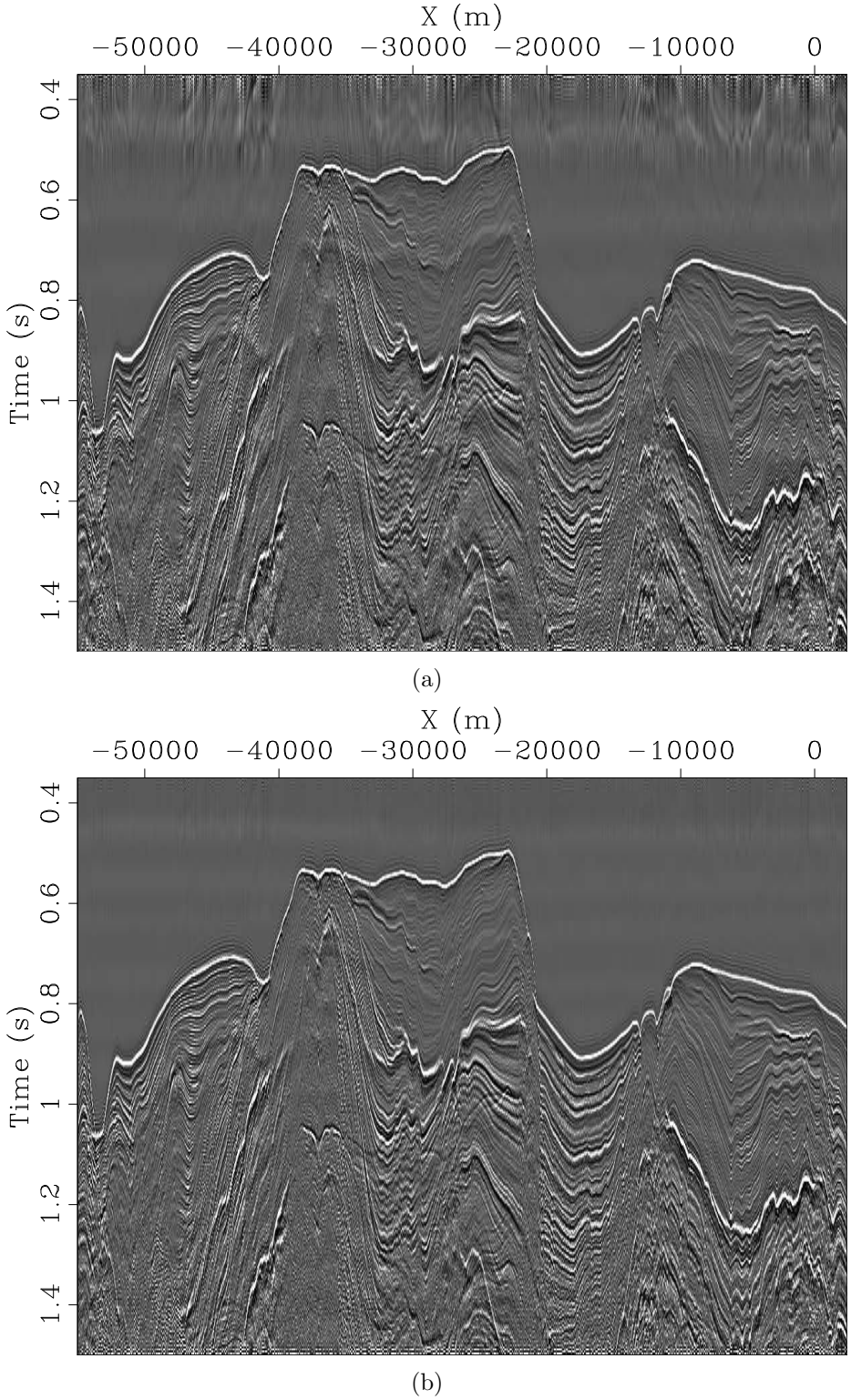

Figure 3: Deconvolution of the 180m offset only. (a) gained input deconvolution with regularization. (b) gained output deconvolution with regularization. Compared to Figures 2(a) and 2(b), the precursors are weaker and the bubble is better handled. In (b) there is less noise than in (a). [**ER**]

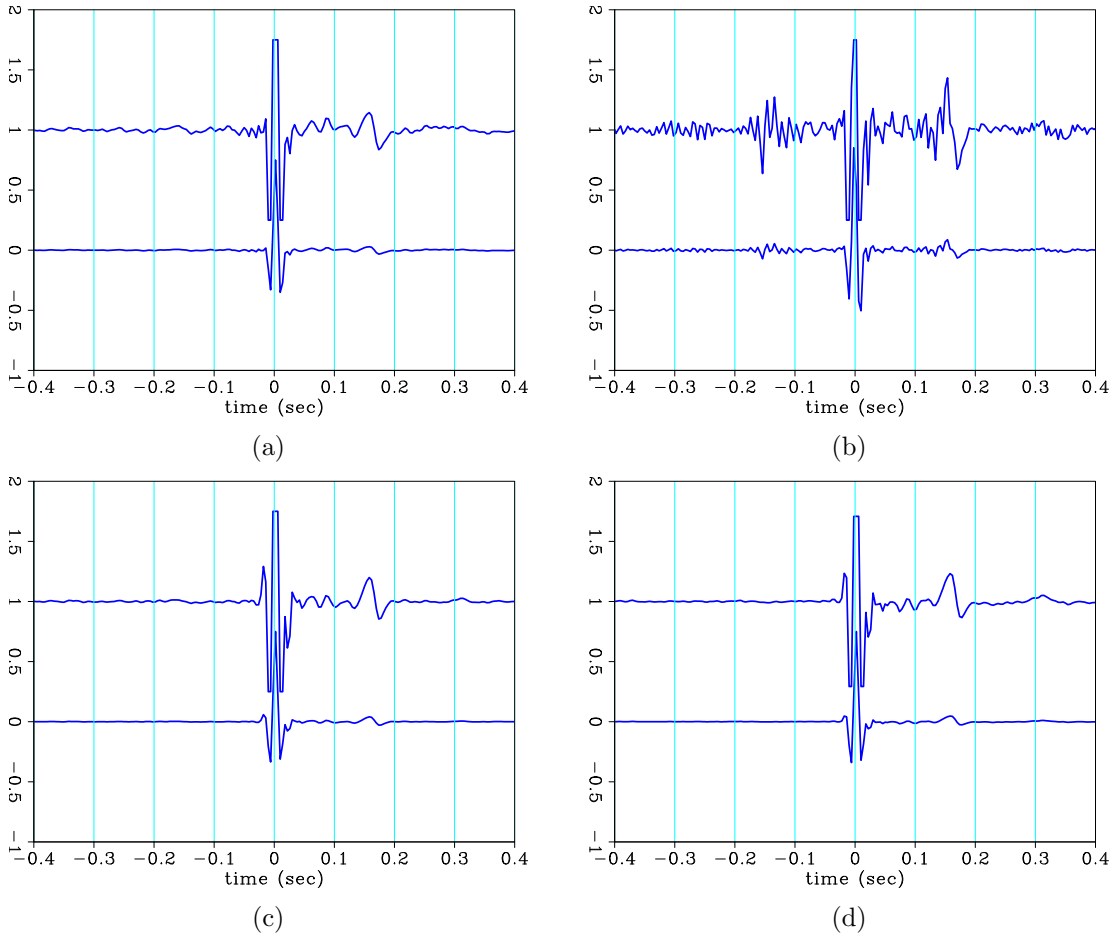

Figure 4: Estimated shot waveforms resulting from inversion using near offset data only. In each graph, the lower trace is unclipped, and the upper trace is clipped to enhance the small coefficients. (a) Gained input decon without regularization (link to figure 2). (b) Gained output decon without regularization. (a) and (b) are the shot waveforms, and their inverses are those that generated Figures 2(a) and 2(b) after deconvolution. Note how much more energy is in the anti-causal part of the shot waveform in (b) compared to (a). (c) Gained input decon with regularization. (d) Gained output decon with regularization. (c) and (d) are shot waveforms, the inverses of which generated Figures 3(a) and 3(b) after deconvolution. [**ER**]

inversion to produce the sparsest output does not result in the correct shot waveform. The interpretation of these results is that the shot waveform varies over this offset range. This change is sufficient to have the inversion produce a shot waveform that *on average* creates the sparsest output when it is deconvolved with the data.

Figure 6(a) is the result of gained input deconvolution with regularizations on the offset group. Compared to Figure 5(a), we can see how the polarity of the reflections is now correct, and also that the precursor is weaker. The bubble however, has not been eliminated.

Figure 6(b) is the gained output deconvolution with regularizations. For this figure, we see spiking with the correct polarity. The precursors are much weaker than the gained input result in Figure 6(a). The bubble has been strongly attenuated, though not as well as in Figure 4(d).

Figures 7(c) and 7(d) are the estimated shot waveforms of the regularized gained input and gained output deconvolutions, respectively. The central Ricker wavelet is almost identical between them, but there are slight differences in the estimated bubble. There is just a hint of stronger anti-causal coefficients in Figure 7(c). Observing the obvious differences in the decon results, we can see why these slight differences are important.

EFFECTS OF DECON ON SPECTRUM

Synthetic test notch elimination

The frequency notch of marine data is an attribute of the acquisition system. We wish to test whether this deconvolution removes the frequency notch under "perfect" conditions. For this purpose, a synthetic wavelet was constructed of three spikes, so as to resemble a Ricker wavelet. The time difference between the lobes are such that they simulate a situation where the source and receivers were at a depth of 9m. The wavelet itself is nearly zero-phase, the spikes having the values $[-1, 2, -0.99]$.

Figure 8(a) is the wavelet, and Figure 8(b) is its amplitude spectrum. The notch is at 83Hz. The regularized deconvolution was applied to this trace. In Figure 8(c) is the estimated shot waveform, and Figure 8(d) is its spectrum. The waveform resembles the synthetic trace, but its first negative lobe is slightly smaller than the second negative lobe, and it has small anti-causal and causal coefficients. Its spectrum is similar in shape, with the notch at the correct frequency. However it does not go to zero at the zero frequency, or at the notch frequency, as in the synthetic trace spectrum.

Figure 8(e) is the deconvolution result. Though the correct lobe has been spiked, there are strong precursors. It appears that the deconvolution has constructed some low frequencies that were absent from the data. In Figure 8(f) we can see that the notch frequency has not been filled as such, but rather that the other frequencies have

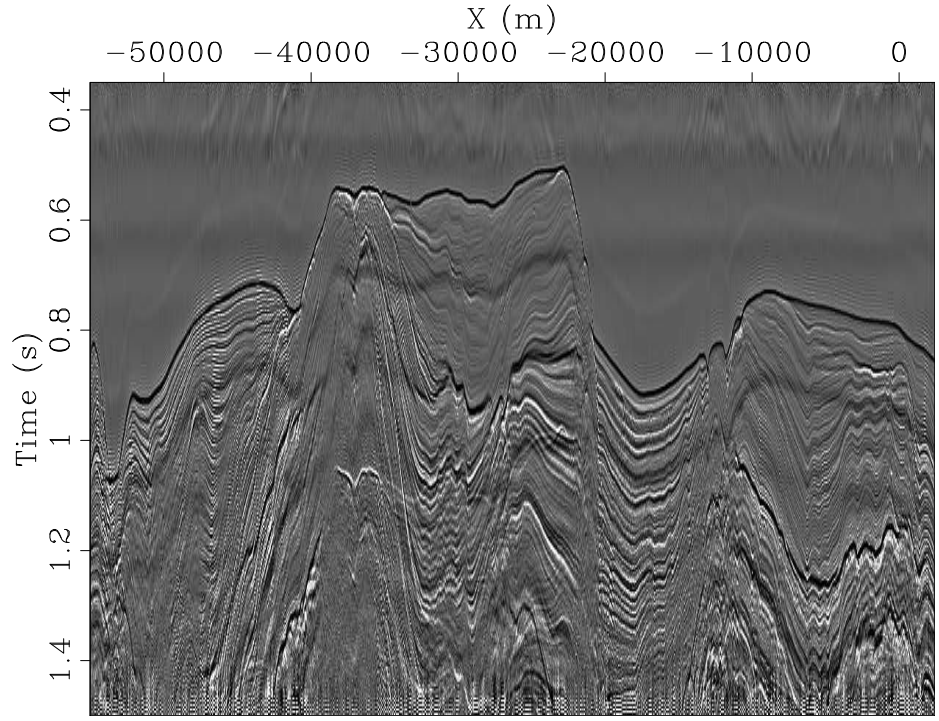

(a)

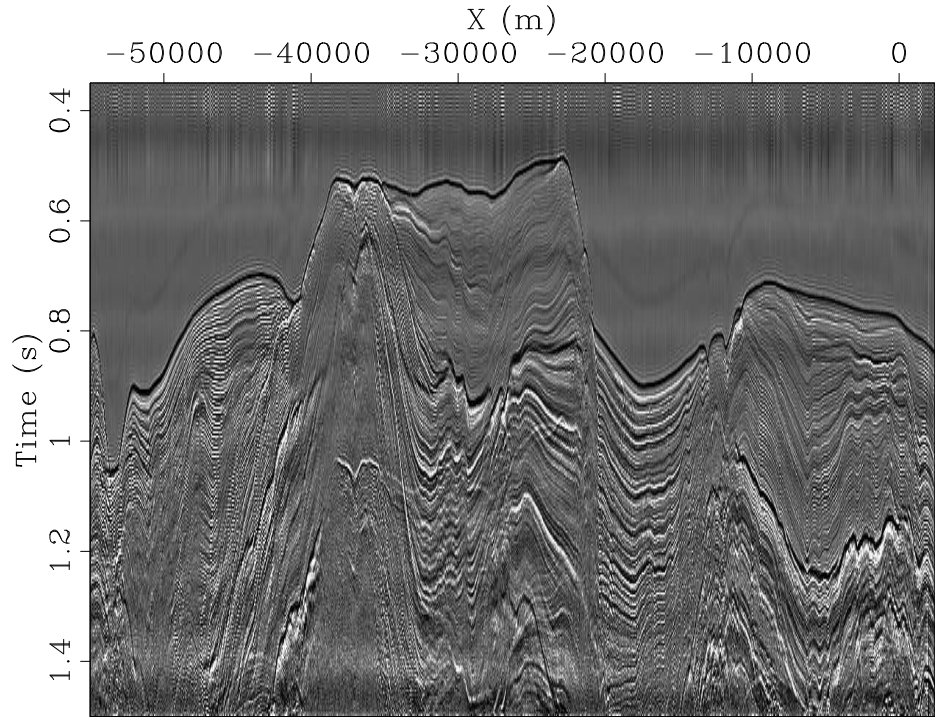

(b)

Figure 5: Deconvolution of offset group (180m - 1180m). (a) Gained input deconvolution without regularization. (b) Gained output deconvolution without regularization. The deconvolution was applied to all offsets in the range, but only the 180m offset deconvolution result is displayed. Note that the wavelet was spiked on a negative lobe. The bubble is still prominent, and there are strong low-frequency precursors in the water. [**ER**]

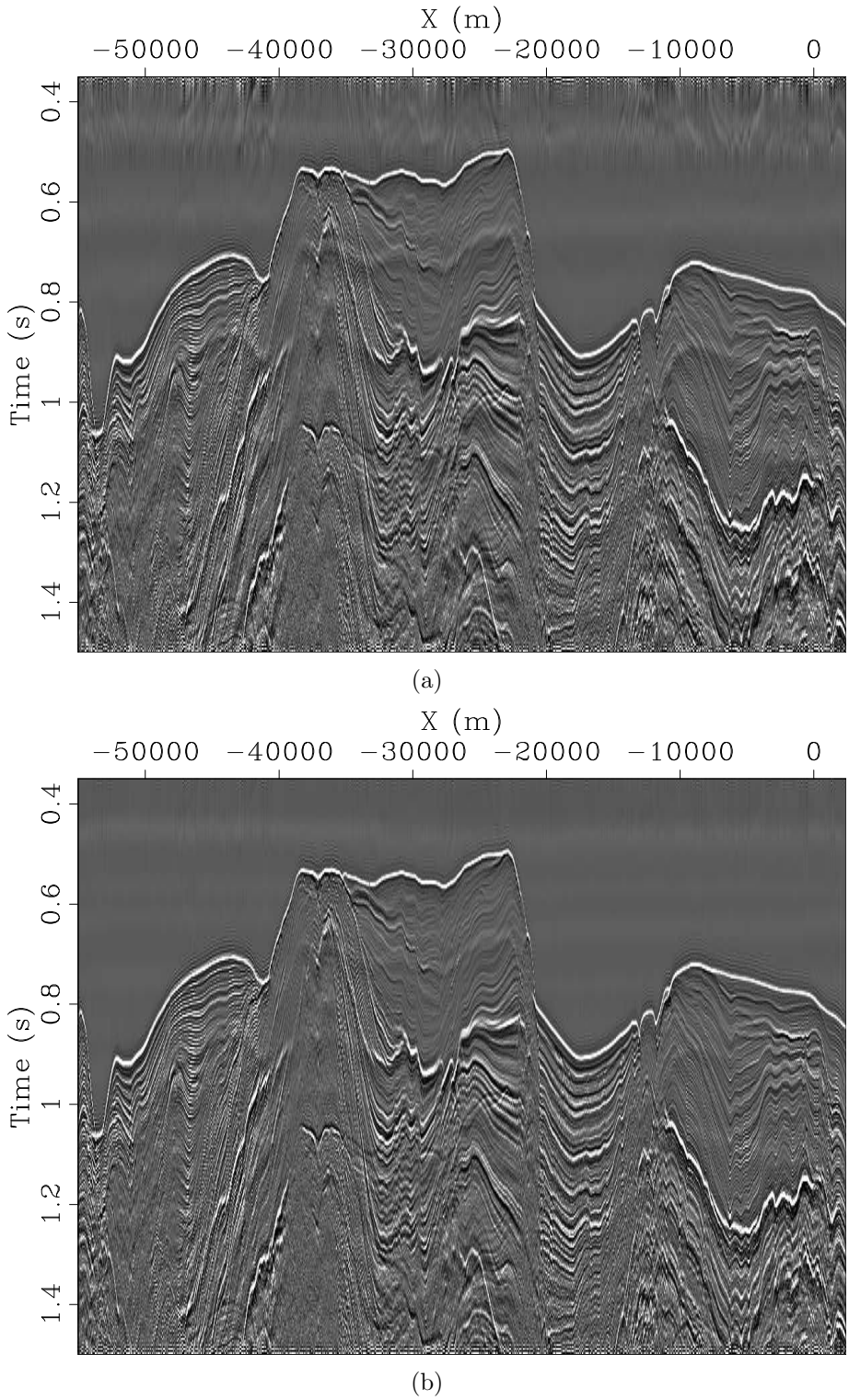

Figure 6: Deconvolution of offset group (180m - 1180m). (a) gained input deconvolution with regularization. (b) gained output deconvolution with regularization. The deconvolution was applied to all offsets in the range, but only the 180m offset deconvolution result is displayed. Note how with regularization, both have been spiked on the central positive lobe of the Ricker wavelet. The precursors have been removed. The bubble is better removed in (b). [**ER**]

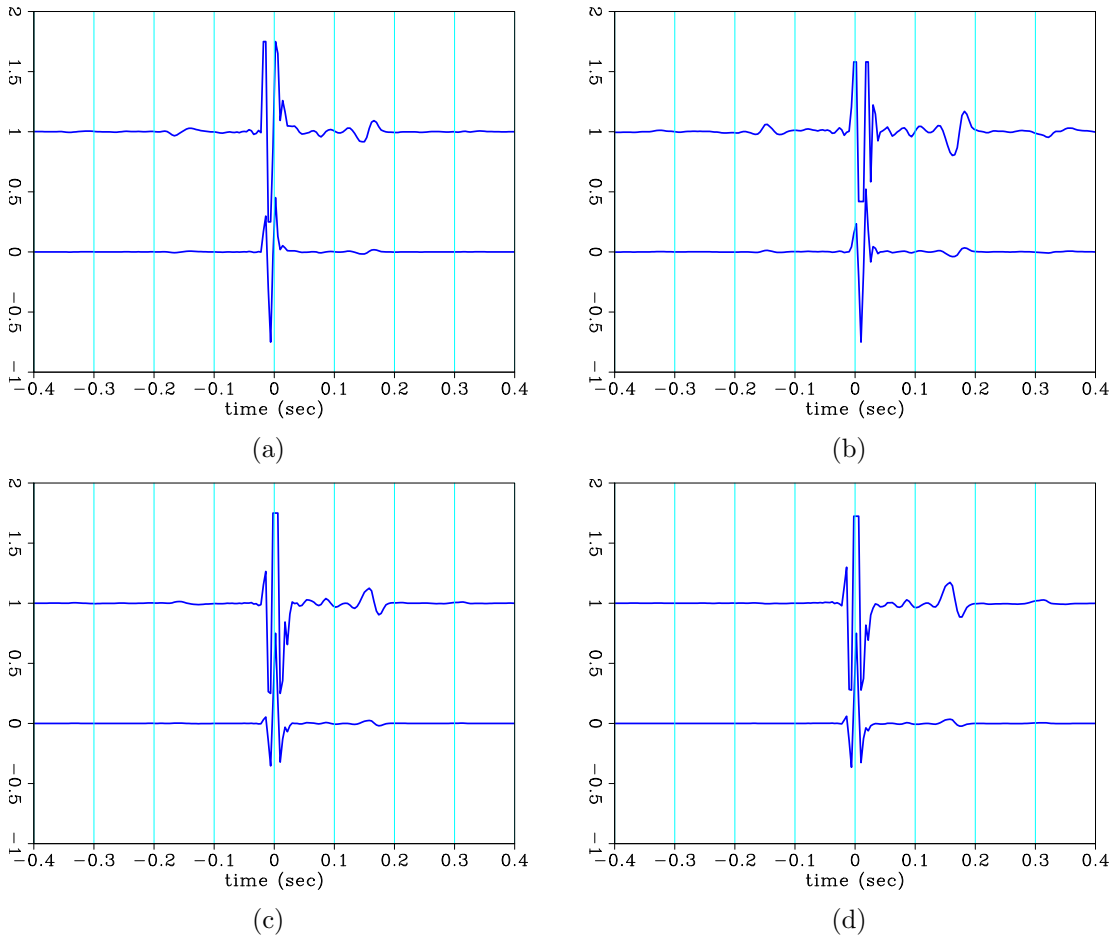

Figure 7: Estimated shot waveforms resulting from inversion using offset group. In each graph, the lower trace is unclipped, and the upper trace is clipped to enhance the small coefficients. (a) Gained input decon without regularization. (b) Gained output decon without regularization. (a) and (b) are shot waveforms, the inverses of which generated Figures 5(a) and 5(b) after deconvolution. In both cases, the main lobe has the wrong polarity. In (a) it is before zero-lag, and in (b) it is after zero-lag. (c) Gained input decon with regularization. (d) Gained output decon with regularization. (c) and (d) are shot waveforms, the inverses of which generated Figures 6(a) and 6(b) after deconvolution. Note how regularization helped to generate a more correct shot waveform, with much weaker precursors. [**ER**]

been decreased so as to equalize the spectrum. The notch frequency of this waveform does not have zero energy, however.

Field data notch elimination

Before applying deconvolution, it is useful to check which frequencies are in the data, as some frequencies may have been filtered out in preprocessing, or were simply not acquired. We also need to test if the notch is apparent in the data, as we expect the deconvolution to remove it. If the source and receivers are deep enough, we will be able to see the notch with the 4ms data we usually have. For the Baja dataset, the source and receivers were at a depth of about 9m, putting the theoretical notch frequency for zero offset at 83Hz, and therefore visible at the data's sampling rate of 4ms.

Figure 9(a) is part of a single near-offset trace, which contains the direct arrival and some of the bubble reverberations. There is no "geology" in the part of the recording, only the effective source signature. Figure 9(b) is the log of the frequency spectrum of this time series. We can see that the very low frequencies have either not been acquired or have been filtered. The bubble harmonics are apparent starting from 6.5Hz at intervals of about 6-7Hz. The source notch is apparent around 113Hz.

Figure 10(a) is the same near-offset trace with the addition of some reflection data. Figure 10(b) is the log spectrum of the entire trace. The notch now appears at around 103Hz. This notch is the result of the combined source and receiver ghosts, which have time delays pertaining to the receivers' and sources' depths in the water, and their offsets. Figures 11(a) and 11(b) are a single shot gather and its log spectrum. The notch starts from around 90Hz in the near offset, and increases in frequency with increasing offset, as illustrated by equation 4.

Figure 12(a) shows the log spectrum of the near-offset section shown in Figure 1. Especially apparent is how the frequency notch moves about the spectrum, from 90Hz to 110Hz. We interpret this as the result of the changing depths of the airgun and the receivers, as they are towed behind the acquisition vessel in the sea. Figure 12(b) is the log spectrum of the regularized gained input deconvolution result, and Figure 12(c) is that of the gained output deconvolution result.

These figures show some additional considerations which are useful for understanding the data, and can aid in evaluating the deconvolution results. In this case, we know that the inversion cannot work perfectly, since the lowest frequencies are not present. We also know that the notch is not at a constant frequency, and therefore the shot waveform is necessarily not constant along the entire near-offset section. We can also see that the deconvolution with the current regularizations is only mildly successful in removing the acquisition frequency notch.

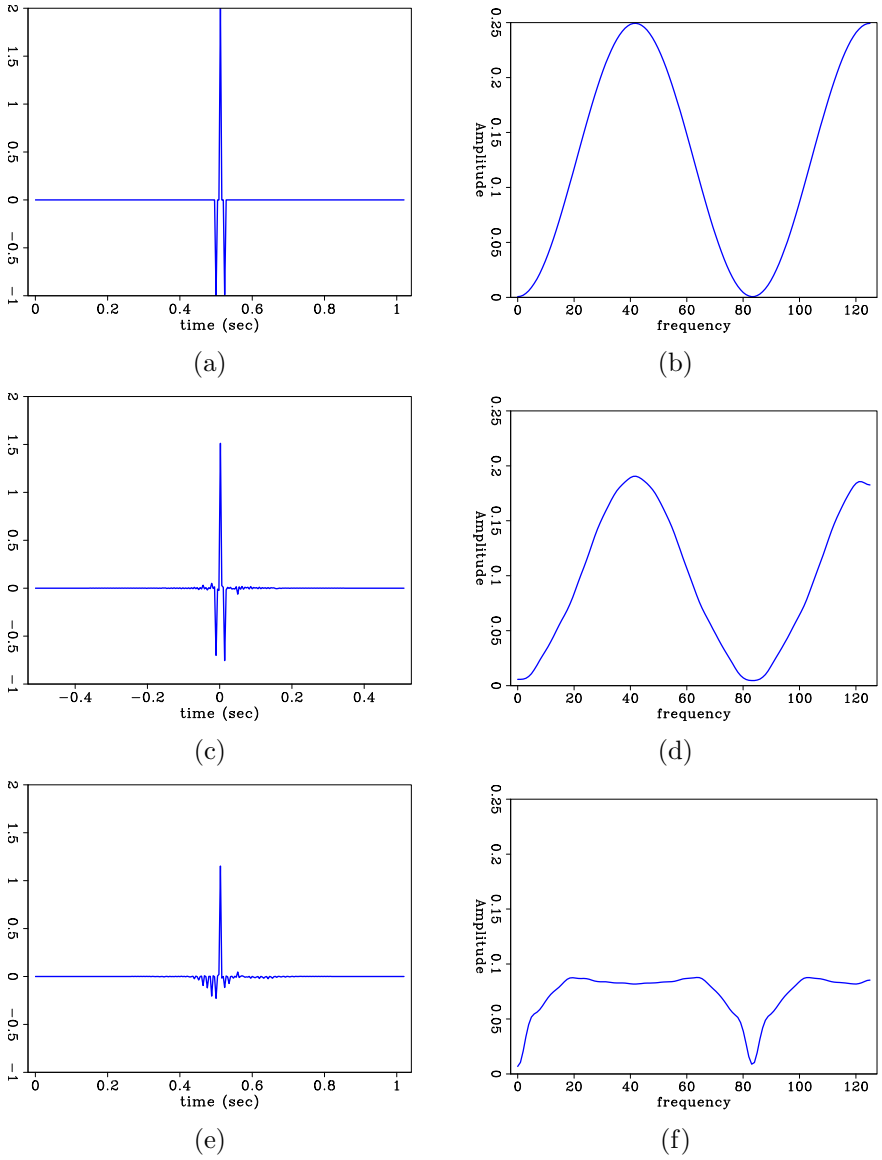

Figure 8: (a) Input trace. (b) Spectrum of input trace. Note the notch at zero and 83Hz (c) Estimated shot waveform from deconvolution. (d) Spectrum of estimated shot waveform. Note how the notch frequencies have some energy. (e) Deconvolved trace. The deconvolution has added some low frequency noise. (f) Spectrum of deconvolved trace. [**ER**]

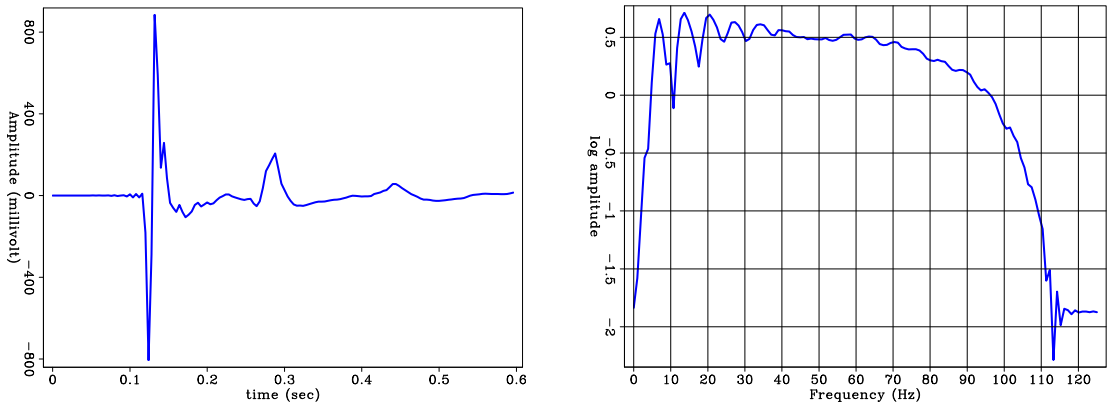

(a) (b)

Figure 9: One near offset trace. (a) Direct arrival and bubble. (b) Log of spectrum of direct arrival and bubble. [**ER**]

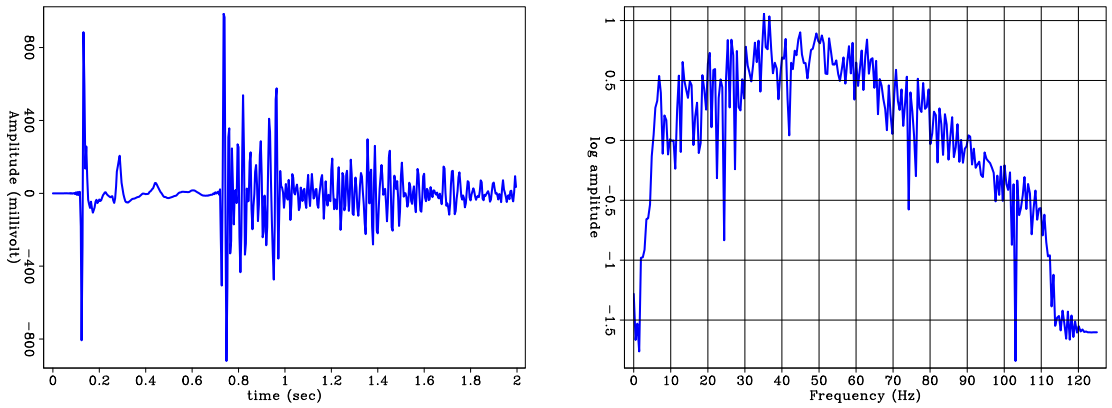

(a) (b)

Figure 10: One near offset trace. (a) Direct arrival, bubble and reflections. (b) Log of spectrum of direct arrival, bubble and reflections. [**ER**]

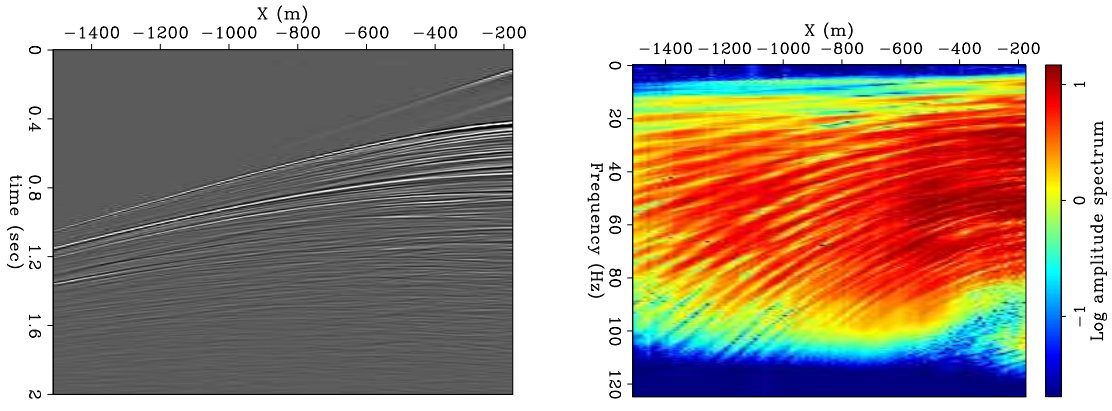

(a) (b)

Figure 11: (a) Shot gather for shot at x=-62850 (b) Log of spectrum of shot gather, showing the notch frequency at around 90Hz at near offsets. [**ER**]

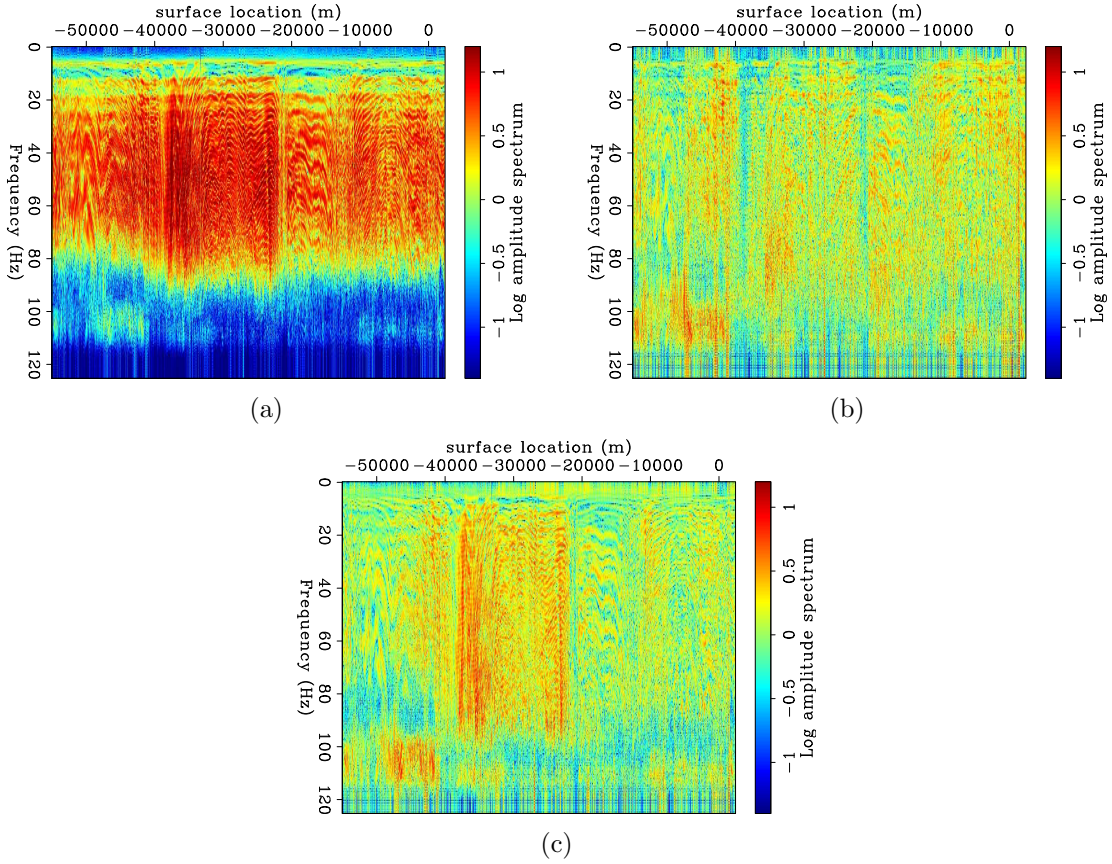

Figure 12: (a) Log spectra of near offset section. (b) Log spectra of gained input decon. (c) Log spectra of gained output decon. Note the notch in (a) and how it changes frequency with surface location, which is a result of perturbations in the source and receiver depths as they are towed behind the vessel. The notch is better filled in (b), but it appears to be filled by some noise generated by the deconvolution itself, just as in Figure 8(e). [**ER**]

DISCUSSION AND CONCLUSION

The inversion optimizes for sparsity, since we assume that geology is sparse, but that requirement alone is not enough. We assume that in a particular marine survey, a single effective shot waveform was used to record all data, and therefore a single filter should be sufficient to deconvolve the entire dataset. The question is how much does that assumption stand up to reality. When considering increasing offsets the recorded waveform may change, and the data is likely to contain not just specular reflections but refractions as well. If there is a significant difference between effective shot waveforms within a survey, the inversion may estimate a shot waveform that produces the best average result for the input data it was given. However, this result may not be very useful for any particular trace in the data. This indicates that we should estimate the shot-waveform only from near-offset data.

The symmetry and filter length regularizations enable us to shape the desired shot waveform to our expectation: a Ricker wavelet, with some bubble reverberations trailing after it. These regularizations help in arriving at a useful result even when the shot waveform varies, such as when we use many offsets. They are easy to implement in the lag-log domain.

Instead of applying the deconvolution to a constant offset or to a multiple offset section, within which the shot waveform can change as a result of different angles of incidence, it may be preferable to apply it to data sorted by angles of incidence. For specular reflections of the same incidence angle, we can assume that the waveform is constant. Therefore, one possibility is to transform the data to the $\tau - p$ domain, and run the deconvolution on constant ray-parameter slices.

The source and receiver depths can change over the acquisition line, and therefore the effective shot waveform and its associated frequency notch may change at each shot. One way of evaluating the success of the deconvolution is in testing how it deals with the frequency notch. We would like to see the notch removed from the data, but we do not want the inversion to fill it with noise. A further avenue of research is to add the notch elimination as a parameter into the inversion.

It is important to check whether the low frequencies were filtered out in preprocessing. This will affect the result since the inversion may compensate by generating low frequencies that have nothing to do with the geology. Also, the filtering may affect the source wavelet, meaning that the Ricker we see is as much a result of preprocessing as it is of the acquisition.

Another conclusion is that success of this deconvolution method is on a dataset by dataset basis. How it functions depends on the data characteristics, and the variability of the shot waveform over traces. Considering the regularization parameters, we cannot conclude from one dataset what set of parameters will work on another.

REFERENCES

Claerbout, J., Q. Fu, and Y. Shen, 2011, A log spectral approach to bidirectional deconvolution: SEP-Report, **143**, 297–300.

Claerbout, J., A. Guitton, and Q. Fu, 2012, Decon in the log domain with variable gain: SEP-Report, **147**, 313–322.

Lizzaralde, D., G. Axen, G. Kent, J. Fletcher, A. Gonzalez, A. Harding, S. Holbrook, and P. Umhoefer, 2002, PESCADOR seismic experiment. funding agency: NSF. data set accessed 20 July 2012 at http://www.ig.utexas.edu/sdc/.

Zhang, Y., J. Claerbout, and A. Guitton, 2011, A new bi-directional sparse/spike deconvolution method that overcomes the minimum phase assumption: 73th EAGE Conference and Exhibition Extended Abstract, F001.